Energy 213 (2020) 119005

Contents lists available at ScienceDirect

Energy

journal homepage: www.elsevier.com/locate/energy

Energy performance prediction of the centrifugal pumps by using a hybrid neural network

Renfang Huang [a, b], Zhen Zhang [a, b], Wei Zhang [c], Jiegang Mou [d], Peijian Zhou [d, *], Yiwei Wang [a, b, **]

[a] Key Laboratory for Mechanics in Fluid Solid Coupling Systems, Institute of Mechanics, Chinese Academy of Sciences, Beijing, 100190, China
[b] College of Engineering Science, University of Chinese Academy of Sciences, Beijing, 100049, China
[c] Science and Technology on Water Jet Propulsion Laboratory, Shanghai, 200011, China
[d] School of Measurement and Testing Engineering, China Jiliang University, Hangzhou, 310018, China

ARTICLE INFO

Article history:
Received 13 February 2020
Received in revised form
26 August 2020
Accepted 2 October 2020
Available online 5 October 2020

Keywords:
Centrifugal pump
Energy performance
Loss model
Physics-informed neural network

ABSTRACT

It is of great significance to rapidly and accurately predict the energy performance of centrifugal pumps for the macro-control of the entire electric power system. However, some challenges are encountered, for example, the numerical simulation requires huge computing resources and calculating time, the theoretical loss model needs to improve the prediction accuracy, etc. Based on the multiple geometrical parameters and operation conditions, a hybrid neural network is proposed to predict the energy performance (i.e. the head, power and efficiency) of centrifugal pumps, where the theoretical loss model is incorporated into the back propagation neural network and then the neural network structure is optimized by automatically determining the node number of hidden layers. When compared with the experiments, the energy performance is well predicted by using the hybrid neural network with the mean-square-error (MSE) for the head, power and efficiency of 0.0062, 8.4E-4, 0.020, respectively. Besides, by considering the theoretical loss model, the hybrid neural network demonstrates a dramatic decrease in the head MSE and the efficiency MSE when compared with the original neural network. Furthermore, the hybrid neural network performs much better than the traditional linear regression in a wide flow-rate range for multiple centrifugal pumps.

1. Introduction

With the rapid development of the global economy, the demand for energy supply is gradually increasing. Although people are vigorously exploiting and utilizing the natural resources on earth, especially the non-renewable energy (i.e. coal, oil, natural gas, etc.), the contradiction between energy supply and demand becomes more and more prominent. It is believed that we need to break through two key issues in order to achieve the sustainable energy development. One is developing new renewable energy such as wind energy, geothermal energy and ocean energy; and the other is making our utmost effort to conserve energy and reduce emissions.

In the whole energy framework, centrifugal pumps play a significant role which can transport the fluid to a specified place by converting the mechanical energy from the prime mover into the fluid pressure energy and kinetic energy. It is widely applied in petrochemicals, nuclear power generation, irrigation, urban water supply and heating systems. Take the Austrian district heating networks for example, the centrifugal pumps provide over 15 TWh heat for around 26% of buildings in 2017 [1]. Besides, centrifugal pumps make contributions to the reliability and efficiency of the electric power system by controlling voltage [1], reducing peaks [2], managing congestion [3] and reserving excess energy [4].

Therefore, it is urgent to rapidly predict the energy performance of centrifugal pumps from the perspective of macro-controlling the entire electric power system. A large number of efforts have been made to study the energy performance for different types of pumps [5–9]. With the rapid development of computer science and technology, computational fluids dynamics (CFD) is acknowledged as an effective tool to visualize the internal flow features and

* Corresponding author.
** Corresponding author.
E-mail addresses: hrenfang@imech.ac.cn (R. Huang), zhangzhen2@imech.ac.cn (Z. Zhang), waynezw0618@163.com (W. Zhang), mjg@cjlu.edu.cn (J. Mou), zhoupj@cjlu.edu.cn (P. Zhou), wangyw@imech.ac.cn (Y. Wang).

https://doi.org/10.1016/j.energy.2020.119005
0360-5442/

predict the energy performance [10,11]. Gu, Pei [12] studies the clocking position of the pump to improve the energy performance by using incompressible Reynolds-averaged Navier−Stokes equation (RANS), indicating that the maximum difference in the efficiency is 2.61% at the design condition. Nam and Chae [13] develops a numerical simulation model to predict the ground heat exchange rate. The simulation model is coupled with the ground heat transfer, the ground surface heat together with the ground heat exchanger, and the simulated temperature is slightly higher than the experimental one with the average error of 0.57 °C [13]. As an energy-saving device, a large-size ionic wind pump is optimized to meet the expectations by using the numerical simulation with the maximum error of 6.2% when the voltage is 10 kV [14]. However, the accuracy of the numerical simulation is strongly dependent on the expertise of the CFD engineer, as it is sensitive to the mesh quality, the turbulence model and the numerical schemes [15−18], and thus, it is necessary to conduct the validation and verification for each simulation case [19,20]. In addition, although the numerical simulation is feasible to predict the energy performance around the design point, it is difficult to capture the unsteady features at the off-design points, such as the stall, secondary flows together with the pressure pulsations [21−23]. And more importantly, numerical simulation requires huge resources and long calculation time, and this cannot satisfy the requirement of the prediction rapidity during the macro-control of the electric power system.

The theoretical loss models are built to evaluate the energy performance for various pumps by calculating the various losses in each components [24]. This method needs very detailed geometrical parameters and usually be used in the design procedure with the energy performance mostly depending on designer's experience [25]. The head and efficiency are rapidly predicted with a set of loss models by iteratively calculating for S1 and S2 stream surface [26], and good agreement is achieved between the predicted and experimental values with the maximum error of 15% [27]. Barbarelli, Amelio [28] develops a one-dimensional numerical code to estimate the energy performances of centrifugal pumps used as turbines in a wide range of specific speed from 9 to 65 rpm$\cdot$m$^{3/4}\cdot$s$^{-1/2}$, and the estimation error is from 5 to 20%. To extend the prediction capability at off-design conditions, the incidence loss and throat flows are suggested to be considered in the mean-line performance prediction method [29]. An experimentally validated optimization routine is proposed by Singh and Nestmann [30] to predict the turbine mode characteristics of a pump, and the errors for all of the centrifugal pumps can fall within ±4% in the full load operating range. From the above, the theoretical loss model is an effective tool for the energy performance prediction, but its prediction accuracy still needs to be improved.

Recently, machine learning has gradually attracted an increasing attention due to its outstanding achievements in various applications, like the image identification, the speech recognition, especially the AlphaGo. Machine learning is a data-driven method, including the genetic algorithm (GA) [31,32], the neural network (NN) [33,34], etc. Hinton and Salakhutdinov [35] reports that high-dimensional data can be converted to low-dimensional codes by training a multilayer neural network with a small central layer to reconstruct high-dimensional input vectors. Therefore, many studies have been made to simulate the complex turbulent flows by using the machine learning. Tracey, Duraisamy [36] develops a machine learning algorithm to construct a stochastic model of the error of low-fidelity models using information from higher-fidelity data sets, and this methodology can provide better approximations of uncertain model outputs and generate confidence intervals. The deep neural network (DNN) method combined with regularization is constructed to simulate in the channel flow, and the test results show that the regularization can suppress the oscillation and prevent the overfitting [37]. Ling, Kurzawski [38] proposes a neural network architecture which uses a multiplicative layer to embed Galilean invariance into the predicted anisotropy tensor, demonstrating an improved prediction accuracy when compared with the baseline RANS linear and nonlinear eddy viscosity models. In terms of the energy performance evaluation for hydraulic pumps, there are usually three indices, i.e., head, power and efficiency. These indices are not only strongly related to each other, but also highly nonlinear with many geometrical parameters. However, the neural network performs well to rapidly predict the pump hydraulic performance [33,34]. The radial basis neural network (RBNN) is adopted to construct the relationship between the performance indices and the multiple geometrical parameters based on the training data, and this trained RBNN show a good ability to evaluate the energy performance of new samples during the optimization design [39]. Since the neural network is straightforward without depending on the designers' experience, the trained neural network maybe lacks some physics to some extent. Besides, poor network topology may lead to overfitting or under-fitting, but there is no clear principle for the determination of the network topology, which should be discussed from case to case.

To instruct the macro-control of the electric power system, a hybrid neural network is proposed based on the available experiments. Based on the multiple geometrical parameters and operation condition, the theoretical loss model is incorporated into the neural network and the neural network structure is optimized automatically. Details of the proposed methodology are described in Section 3 and Section 4. Section 5 discusses (a) the effects of the neural network structure, (b) the comparisons with the original neural network and (c) the comparisons with the linear regression method. Conclusions are provided in Section 6.

2. Problem description

The centrifugal pump is treated as a typical energy-consuming device in the electric power system. The wide applications of centrifugal pumps benefit from its numerous advantages, i.e., simple and compact structures, easy installation, low maintenance cost, and reliable operations. The centrifugal pump is composed of an inlet pipe, a centrifugal impeller and a volute, as shown in Fig. 1. The main geometrical parameters are described in Fig. 2, including the inlet diameter for the inlet pipe D_0, the inlet diameter for the impeller D_1, the outlet diameter for the impeller D_2, the blade outlet width b_2, the blade outlet angle β_2, the volute throat area F_t, and the blade number z.

It is of great significance to accurately and rapidly evaluate the energy performance for centrifugal pumps. Usually, the energy performance is described by the head H, the power P and the efficiency η. The energy performance is not only strongly affected by the main geometrical parameters described above, but also related to the operation conditions, such as the flow rate Q and the rotational speed n. Additionally, the design flow rate Q_d is usually provided for a specific pump. Therefore, the problem is how to forecast the energy performance based on the seven geometrical parameters and the operation conditions. This paper aims at proposing a hybrid neural network combined with the theoretical loss models and the network structure optimization in order to make up for the deficiency of the traditional data-driven method, that is lacking in some underlying physics.

441 samples are collected from experiments of ten centrifugal pumps. The energy performance tests are conducted on a closed test rig in Shenyang, China, which meets the international standard of ISO9906 and Chinese national standard of GB/T3216. The test accuracy of the experimental device is Level I. The centrifugal pumps are tested at the room temperature with water as the

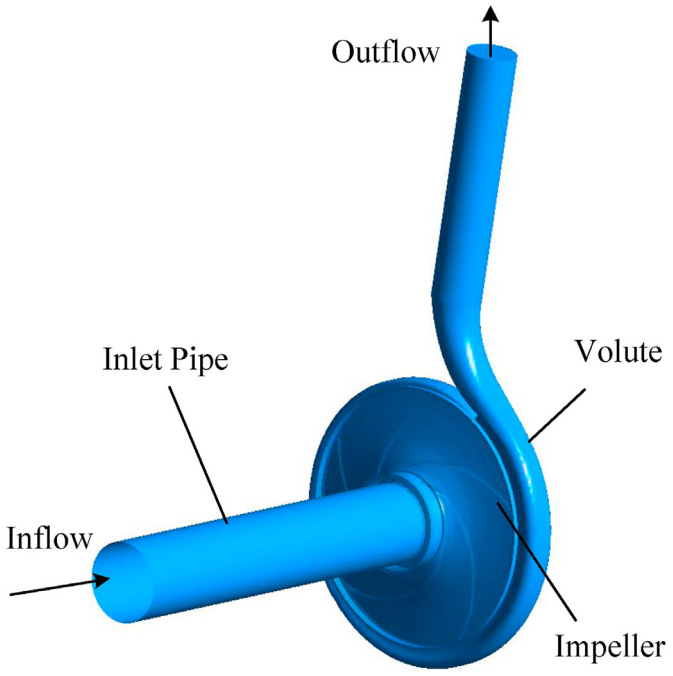

Fig. 1. The centrifugal pump structure including the inlet pipe, the centrifugal impeller and the volute.

experimental medium. The flow rate is measured by an electromagnetic flowmeter; the shaft power is measured by a torque transducer. The pressure is measured by two pressure sensors. One is installed at the upstream of the pump, and the other is installed at the downstream of the pump. Thus, the pump head is calculated by the measured pressure difference. Each pump is operated at various flow-rates, which is controlled by an outlet valve. All of the measured data are processed and saved automatically by a data acquisition system.

3. Theoretical loss model of energy prediction

3.1. Theoretical head

Based on the Euler equation, the theoretical head $H_{t\infty}$ for an ideal fluid as it passes through an infinite multi-blade impeller,

$$H_{t\infty} = \frac{1}{g}(u_2 v_{2u\infty} - u_1 v_{1u\infty}) \tag{1}$$

where subscript 1 and 2 presents the impeller inlet and outlet, respectively; subscript ∞ denotes the value is calculated on the assumption that the blade number is infinite and the blade thickness is infinitely thin, so the fluid is strictly flowing along the blade shape and the flow angle is equal to the blade angel; g is the acceleration of gravity, $= 9.81$ m/s^2; u is the circumferential velocity of impeller; $v_{u\infty}$ is the circumferential component of absolute velocity v_∞.

In general, $v_{1u\infty}$ is assumed to be zero under the axial inflow condition, and then the theoretical head can be simplified as

$$H_{t\infty} = \frac{u_2 v_{2u\infty}}{g} \tag{2}$$

In practice, the impeller blade is finite number (usually 4–7) with a certain thickness. In the flow passage of the finite blade impeller, the relative velocity would slip at the impeller outlet due to the inertia of the fluid, as shown in Fig. 3, where w is the relative velocity, subscript m denotes the meridional component. It is noted that velocity slip phenomenon indicates the energy transferred to the fluid by the rotating impeller is decreased. Therefore, the slip effect is considered by calculating the difference for the circumferential component of absolute velocity between the infinite blade condition and finite blade condition,

$$\Delta v_{2u} = v_{2u\infty} - v_{2u} \tag{3}$$

The slip factor σ is defined in equation (4) to evaluate the slip effect, which is the key to calculate the theoretical head.

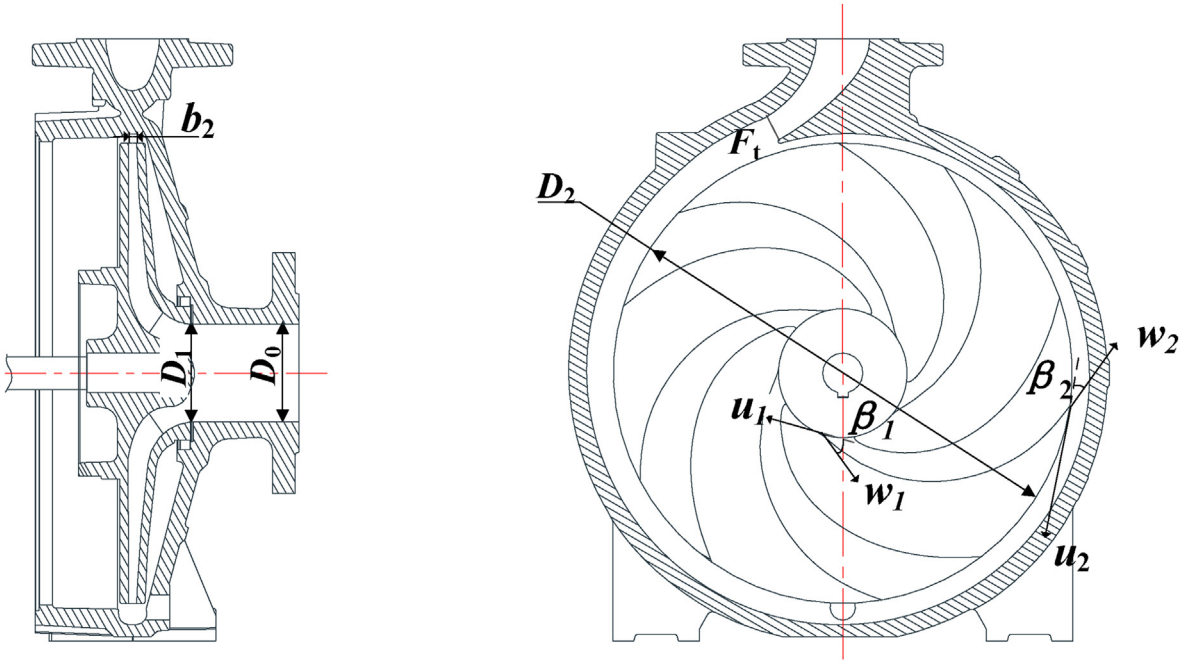

Fig. 2. Geometrical parameter diagram of a centrifugal pump.

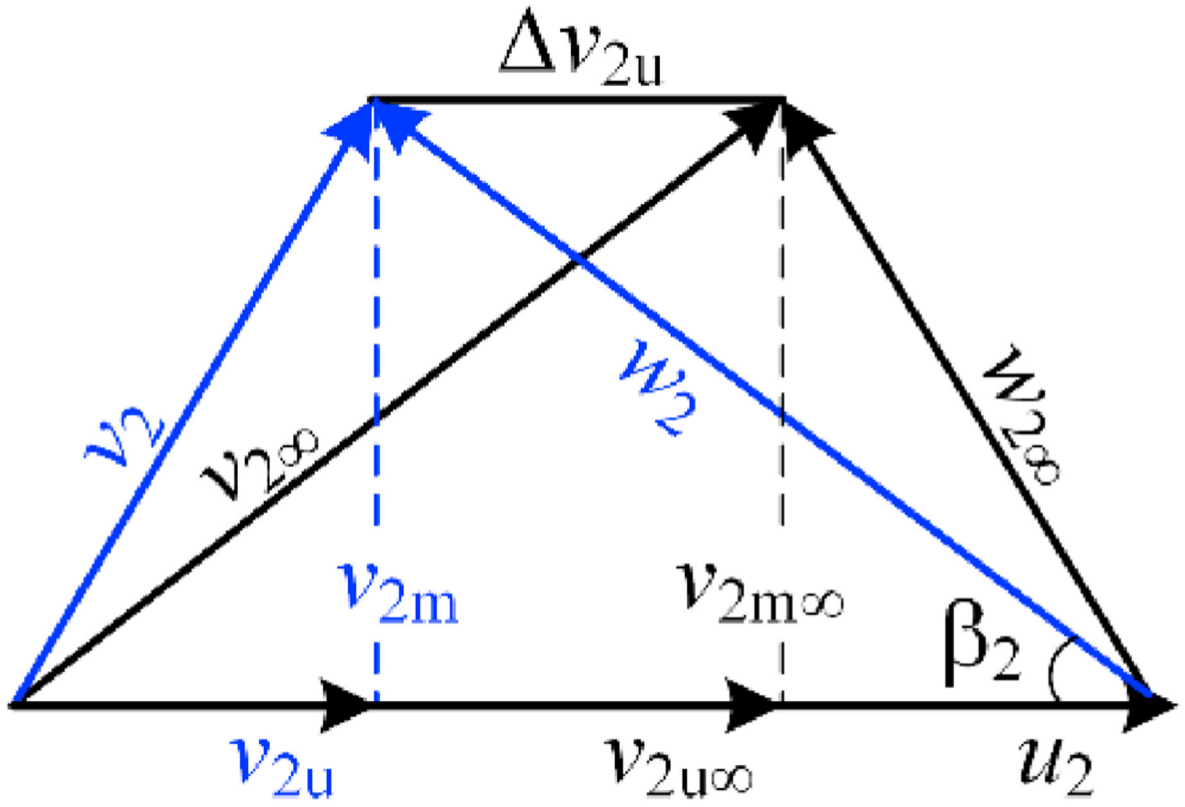

Fig. 3. Velocity triangle at the impeller outlet demonstrating the slip phenomenon.

$$\sigma = \frac{u_2 - \Delta v_{2u}}{u_2} = 1 - \frac{\Delta v_{2u}}{u_2} \tag{4}$$

Many investigations are made to improve the σ formula [40–43]. Based on large experimental data for centrifugal pumps, Liu, Tan [44] studies different formulas for the slip factor, and the Wiesner equation is introduced herein to calculate the slip factor as shown in equation (5). Thus, the theoretical head is derived by regression analysis with a calculation coefficient k given in equations (6) and (7), where the coefficient ψ_2 is denoted as 0.8 for the volute centrifugal pumps, n_s is the specific speed.

$$\sigma = 1 - \frac{\sqrt{\sin \beta_2}}{z^{0.7}} \tag{5}$$

$$H_t = \frac{u_2}{g}\left(k\sigma u_2 - \frac{Q}{3600\pi D_2 b_2 \psi_2 \tan \beta_2}\right) \tag{6}$$

$$k = \begin{cases} 1.009\left(1 - e^{-0.088 n_s}\right), & 30 < n_s < 65 \ \grave{} n \geq 2000\text{r/min} \\ 0.71\left(\frac{n_s}{100}\right)^3 - 2.58\left(\frac{n_s}{100}\right)^2 + 2.91 \times \frac{n_s}{100} + 0.00726, & n_s \geq 65 \ \grave{} n \geq 2000\text{r/min} \\ 1.036\left(1 - e^{-0.06 n_s}\right), & n_s > 65 \ \grave{} n < 2000\text{r/min} \end{cases} \tag{7}$$

3.2. Loss in the inlet pipe

Before the fluid enters into the centrifugal pump impeller, a hydraulic loss occurs in the inlet pipe, which is calculated by equation (8). In general, the velocity field is relatively uniform, so this loss is small, especially under the design condition.

$$\Delta h_{suc} = \lambda \frac{C_0^2}{2g} \tag{8}$$

$$C_0 = \frac{4Q}{\pi D_0^2} \tag{9}$$

where λ is the friction coefficient; C_0 is the axial velocity in the inlet pipe; D_0 is the inlet diameter for the inlet pipe; Q is the flow rate.

Since the Reynolds numbers are of 10^5 magnitudes in the

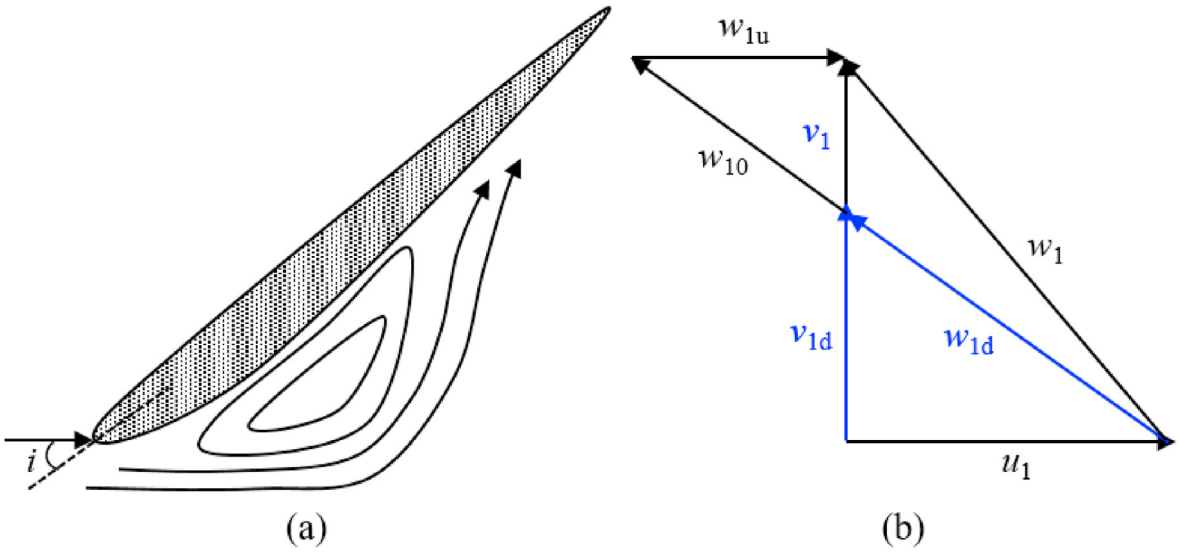

Fig. 4. (a) Schematic diagram of the incidence loss and (b) inlet velocity triangle.

centrifugal pumps, the friction coefficient λ is calculated by equation (10) which is still effective for Re < 10^6 [7].

$$\lambda = \frac{0.3164}{\mathrm{Re}^{0.25}} \tag{10}$$

3.3. Incidence loss in the impeller

The inlet blade angle for a centrifugal pump is determined by meeting the requirement of non-impact inflows at the design flow rate. When the centrifugal pump is operated under the off-design condition, the inlet flow angle is not consistent with the blade angle, causing the flow separation as shown in Fig. 4. The relative velocity at the impeller inlet w_1 is decomposed into w_{10} and w_{1u}. w_{10} is in the same direction as the relative velocity w_{1d} under the design condition. w_{1u} is the imaginary circumference velocity, indicating the incidence level.

Therefore, the incidence loss in the impeller is defined in equation (11), where f_{inc} is the incidence loss coefficient, ranging from 0.5 to 0.7 [26,45].

$$\Delta h_{inc} = f_{inc}\frac{w_{1u}^2}{2g} \tag{11}$$

Based on the velocity triangle in Fig. 4 (b), the w_{1u} can be calculated by equation (12), where Q_d is the design flow rate.

$$\frac{w_{1u}}{u_1} = \frac{v_1 - v_{1d}}{v_{1d}} = \frac{Q - Q_d}{Q_d} \tag{12}$$

Substituting equation (12) into equation (11), the incidence loss finally can be written as follows,

$$\Delta h_{inc} = \frac{f_{inc}}{2g}\left(u_1\frac{Q - Q_d}{Q_d}\right)^2 \tag{13}$$

3.4. Disk friction loss

When the impeller is rotating, the fluid between the shroud and the blades would generate friction and cause hydraulic loss which is termed as disk friction loss ΔP_{df}. For a centrifugal pump, the disk friction loss ΔP_{df} is large and defined as follows,

$$\Delta P_{df} = f_{df}\rho_l D_2^2 u_2^3 \tag{14}$$

$$f_{df} = \begin{cases} \dfrac{0.166875}{\mathrm{Re}_{df}^{0.5}}, \mathrm{Re}_{df} < 3\times 10^5 \\ \dfrac{0.0038875}{\mathrm{Re}_{df}^{0.2}}, \mathrm{Re}_{df} \geq 3\times 10^5 \end{cases} \tag{15}$$

$$\mathrm{Re}_{df} = \frac{\rho_l u_2 R_2}{\mu_l} \tag{16}$$

where f_{df} is the disk friction loss coefficient, Re_{df} is the Reynolds number, ρ_l is the liquid density and μ_l is the liquid dynamic viscosity.

3.5. Actual head, power and efficiency

Based on the previous work [7], the energy is lost during the process of converting input power into the fluid energy. In general, the energy losses for a centrifugal pump are decomposed into the hydraulic loss, the volume loss and the mechanical loss. The hydraulic losses are related to the geometrical structure and operation conditions, including the loss in the inlet pipe Δh_{suc}, incidence loss Δh_{inc}, surface friction loss Δh_{sf}, blade loading loss Δh_{bl}, separation loss Δh_{sep}, wake mixing loss Δh_{mix}, incidence loss in the volute Δh_{Vinc}, friction loss of the volute Δh_{Vsf} and separation loss of the volute Δh_{Vdiff}. The total hydraulic losses Δh_{tol} is defined in equation (17) by summing up all of the losses and the actual head H is the difference between the theoretical head H_t and the total hydraulic losses Δh_{tol} with the definition in equation (18).

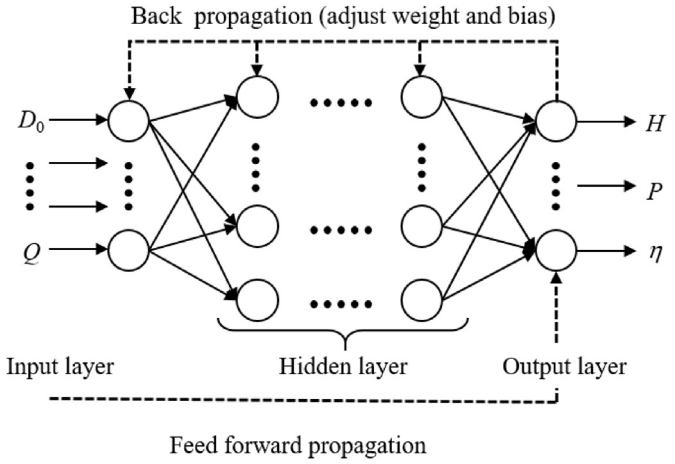

Fig. 5. Diagram of the typical back propagation neutral network (BPNN).

$$\Delta h_{tol} = \Delta h_{suc} + \Delta h_{inc} + \Delta h_{sf} + \Delta h_{bl} + \Delta h_{sep} + \Delta h_{mix} + \Delta h_{Vinc} + \Delta h_{Vsf} + \Delta h_{Vdiff} \tag{17}$$

$$H = H_t - \Delta h_{tol} \tag{18}$$

Besides, additional losses are the recirculation loss ΔP_{rec}, the disk friction loss ΔP_{df}, and the leakage loss ΔP_{lk}. According to the energy conservation, the input power by the prime mover is the sum of the effective power and the additional losses as mentioned above.

$$P = \rho g Q H_t + \Delta P_{rec} + \Delta P_{df} + \Delta P_{lk} \tag{19}$$

Therefore, the total efficiency for a centrifugal pump is determined as follows,

$$\eta = \frac{\rho g Q H}{P} = \frac{\rho g Q [H_t - \Delta h_{tol}]}{\rho g Q H_t + \Delta P_{rec} + \Delta P_{df} + \Delta P_{lk}} \tag{20}$$

$$\begin{aligned} \Delta h_{NN} &= \Delta h_{sf} + \Delta h_{bl} + \Delta h_{sep} + \Delta h_{mix} + \Delta h_{Vinc} + \Delta h_{Vsf} + \Delta h_{Vdiff} \\ \Delta P_{NN} &= \Delta P_{rec} + \Delta P_{lk} \end{aligned} \tag{21}$$

$$\begin{aligned} H &= H_t - \Delta h_{tol} = H_t - (\Delta h_{suc} + \Delta h_{inc} + \Delta h_{NN}) \\ P &= \rho g Q H_t + \Delta P_{df} + \Delta P_{NN} \\ \eta &= \frac{\rho g Q [H_t - \Delta h_{suc} - \Delta h_{inc} - \Delta h_{NN}]}{\rho g Q H_t + \Delta P_{df} + \Delta P_{NN}} \end{aligned} \tag{22}$$

The back propagation neural network (BPNN) is a classic data-driven method including the input layer, the hidden layer together with the output layer as shown in Fig. 5. Firstly, the data samples are classified into three sets, i.e., the training set, the validation set and the test set. The training set is used for the feed forward propagation process by fitting the weights and biases and obtaining an error when compared with the true values, which is termed as training error. The validation set is used to adjust and optimize the weights and biases in the back propagation process and get a validation error every epoch. Once the validation error meets one of the convergence criterions, the BPNN model is finally determined and cannot be tuned any more. The test set is only used to evaluate the generalization capability for the determined BPNN model.

In this paper, the BPNN method is used to assess the energy performance for centrifugal pumps with the modeling data described as $\mathbf{S} = \{\mathbf{X}, \mathbf{Y}\}$, where $\mathbf{X} = \{\mathbf{x_1}, \mathbf{x_2}, \cdots, \mathbf{x_{N-1}}, \mathbf{x_N}\}^T \in R^{N\times 10}$ is the inputs, $\mathbf{Y} = \{\mathbf{y_1}, \mathbf{y_2}, \cdots, \mathbf{y_{N-1}}, \mathbf{y_N}\}^T \in R^{N\times 3}$ is the targets obtained by the experiments, N is the number of sampling data. The i-th sample data set can be expressed in equation (23). It can be clearly seen that there are ten inputs and three outputs in this neural network. Ten inputs are expressed as $\mathbf{x}_i = [D_0(i), D_1(i), D_2(i), b_2(i), \beta_2(i), z(i), F_t(i), Q_d(i), n(i), Q(i)]^T$, i.e. the inlet diameter for the inlet pipe D_0, the inlet diameter for the impeller D_1, the outlet diameter for the impeller D_2, the blade outlet width b_2, the blade outlet angle β_2, the blade number z, the volute throat area F_t, the design flow rate Q_d, the rotational speed n, and the flow rate Q. Three outputs are the energy performance expressed as $\mathbf{y}_i = [H(i), P(i), \eta(i)]^T$, i.e. the head H, the power P, and the efficiency η.

$$\mathbf{s}_i = \left\{ \begin{array}{l} \mathbf{x}_i = [D_0(i), D_1(i), D_2(i), b_2(i), \beta_2(i), z(i), F_t(i), Q_d(i), n(i), Q(i)]^T, \\ \mathbf{y}_i = [H(i), P(i), \eta(i)]^T \end{array} \right\} \tag{23}$$

4. Hybrid neural network

Based on the available geometrical parameters and operation conditions given in Section 2, the loss in the inlet pipe Δh_{suc}, the incidence loss Δh_{inc} and the disk friction loss ΔP_{df} can be computed as described in Section 3. However, the formulas for the other losses are too complex to calculate which are given in the literature [7]. In this paper, a hybrid neural network is developed to evaluate the left losses (i.e., Δh_{NN} and ΔP_{NN} in equation (21)), and finally the energy performance (H, P, η) can be computed by equation (22).

It is widely acknowledged that the neural network structure is of great significance to the BPNN prediction capability. The present neutral network has ten inputs and three outputs, but the node number for the hidden layer is still unknown, which is a very important parameter without a universal and scientific solution. In general, the node number is dependent on the designer's experiences and determined through multiple trials. If the node number for the hidden layer is too small, the BPNN is not able to learn; if the node number is too many, the training error can be reduced to some extent, but it will undoubtedly increase the learning time and may

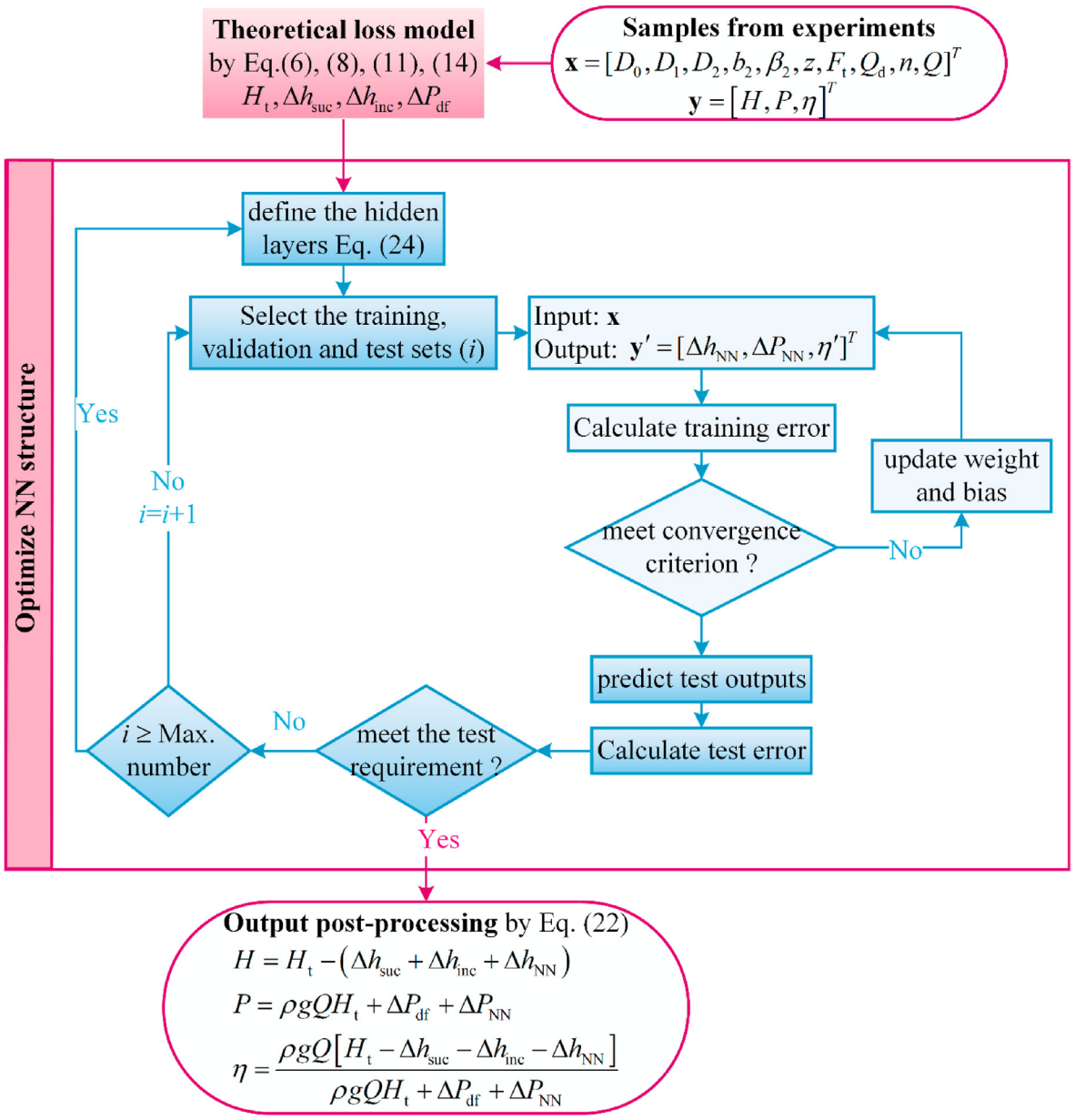

Fig. 6. Hybrid neural network combined with theoretical loss models and network structure optimization.

fall into a local minimum, causing over-fitting phenomenon. Thus, it is necessary to determine an appropriate node number for hidden layers, taking as few nodes as possible to meet the requirement of the learning accuracy. Based on the previous investigations [46,47], the node number in the hidden layer is recommended according to equation (24), where n is the node number of the input layer, $n = 10$; m is the node number of the output layer, $m = 3$; a is a constant ranging from 1 to 10; n_{NN} is the node number of the hidden layer.

$$n_{NN} = \sqrt{n + m} + a \tag{24}$$

The recommended selection region in equation (24) is combined with the classic back propagation neural network and then the theoretical loss model is introduced to constitute the hybrid neural network for the energy performance prediction of centrifugal pumps, as shown in Fig. 6. The detailed process is explained as follows.

Step 1. Collect 441 samples $\mathbf{S} = \{\mathbf{X}, \mathbf{Y}\}$ from the experiments of ten centrifugal pumps and calculate the theoretical head and losses based on the geometrical parameters and operation conditions.

Step 2. Define the node number for the hidden layers by using Eq. (24) with a slightly increasing margin. As a result, the node number for the first hidden layer varies from 4 to 20, and the node number for the second hidden layer varies from 0 to 20.

Step 3. Divide the samples into the training set, the validation set and the test set. 132 samples from 441 samples are treated as the test samples. 85% of the rest 309 samples are treated as the training samples, and 15% of the rest 309 samples are for validation. Save the current learning number as i.

Step 4. Train the network feedforward. The activation function is a hyperbolic tangent transfer function, that is *tansig*, defined as

tansig$(x) = 2/(1+e^{-2x})$-1. For this activation function, the x value can be arbitrary, and the output of the activation function is in the range of $-1 \sim +1$.

Step 5. Assess the capability of the hybrid neural network by using the mean-squared-error (MSE) in equation (25), where j means the j-th performance index (i.e., head, power, efficiency), $y_{i,j}$ is the true value (i.e., the experimental value), $\hat{y}_{i,j}$ is the predicted output, p indicates the number of the current set.

$$\mathrm{MSE}_j = \frac{1}{p}\sum_{i=1}^{p}\left(y_{i,j} - \hat{y}_{i,j}\right)^2, j = 1,2,3 \tag{25}$$

Step 6. Evaluate whether the current network capability meets the convergence criterions, i.e., (1) the validation error is smaller than the preset error, (2) the validation error does not decrease any more during 200 iterations, (3) the epoch reaches the maximum iterations. The process is terminated if any of the convergence criterions is achieved. If no, adjust the weights together with the biases, and go back to Step 4. If yes, continue to the next step.

Step 7. Assess the current network with the test set and calculate the test error using equation (25).

Step 8. Evaluate whether the test error meets the test requirements. If yes, post-process the data by using Eq. (22), and the current neural network is ready to predict the energy performance for new samples. If not, evaluate whether the learning number i is larger than the preset maximum number. If $i <$ maximum number, randomly divide the 309 samples again with 85% for training and 15% for validation, save the learning number as $i = i + 1$, and go back to Step 4. If $i \geq$ maximum number, go back to Step 2, indicating the current test error cannot meet the requirements after multiple attempts and thus it is necessary to adjust the neural network structure.

5. Results and discussions

5.1. Effects of the neural network structure

The neural network (NN) capability is strongly affected by the neural network structure. Based on the empirical formula in equation (24) together with an increasing margin, the node number for the 1st hidden layer varies from 4–20, and the node number for the 2nd hidden layer varies from 0–20. Note that the node number of the 2nd hidden layer is defined as zero, indicating there is only one hidden layer.

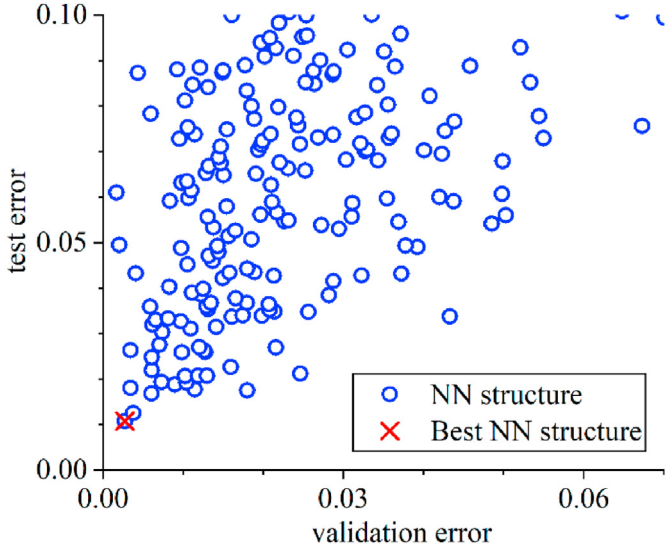

Fig. 7. The validation error and test error for various neural network (NN) structures.

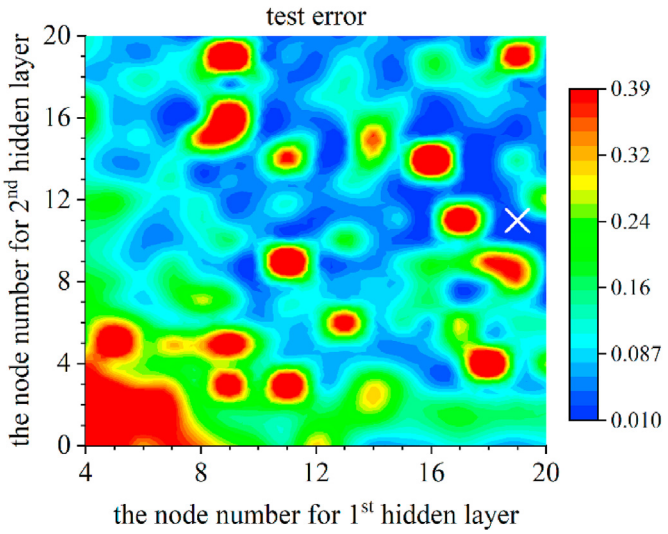

Fig. 8. The test error for various neural network structures with the best neural network structure marked in ×

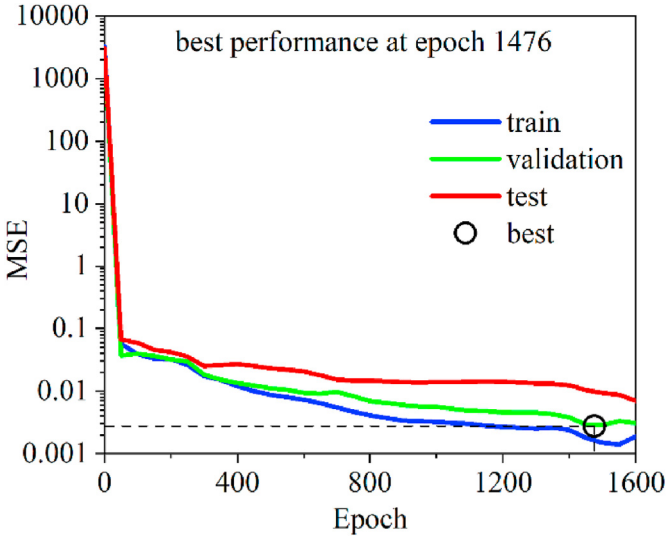

Fig. 9. MSE history during the training, validation, test process.

Although during the learning and testing process as shown in Fig. 6, MSE is used to evaluate the training error, the validation error and the test error. Usually, the training error is smaller than the validation error. The validation error is used to optimize the neural network parameters, and the test error is to assess its generalization capability. The test error and validation error for various neural network structures are shown in Fig. 7. The best neural network structure is marked with red color with the validation error of 0.003 and the test error of 0.01. Moreover, the validation error is generally smaller than the test error at the same neural network structure, indicating that the test error can be treated as a comprehensive evaluation index for the neural network.

Fig. 8 shows the distribution of the test error for various neural

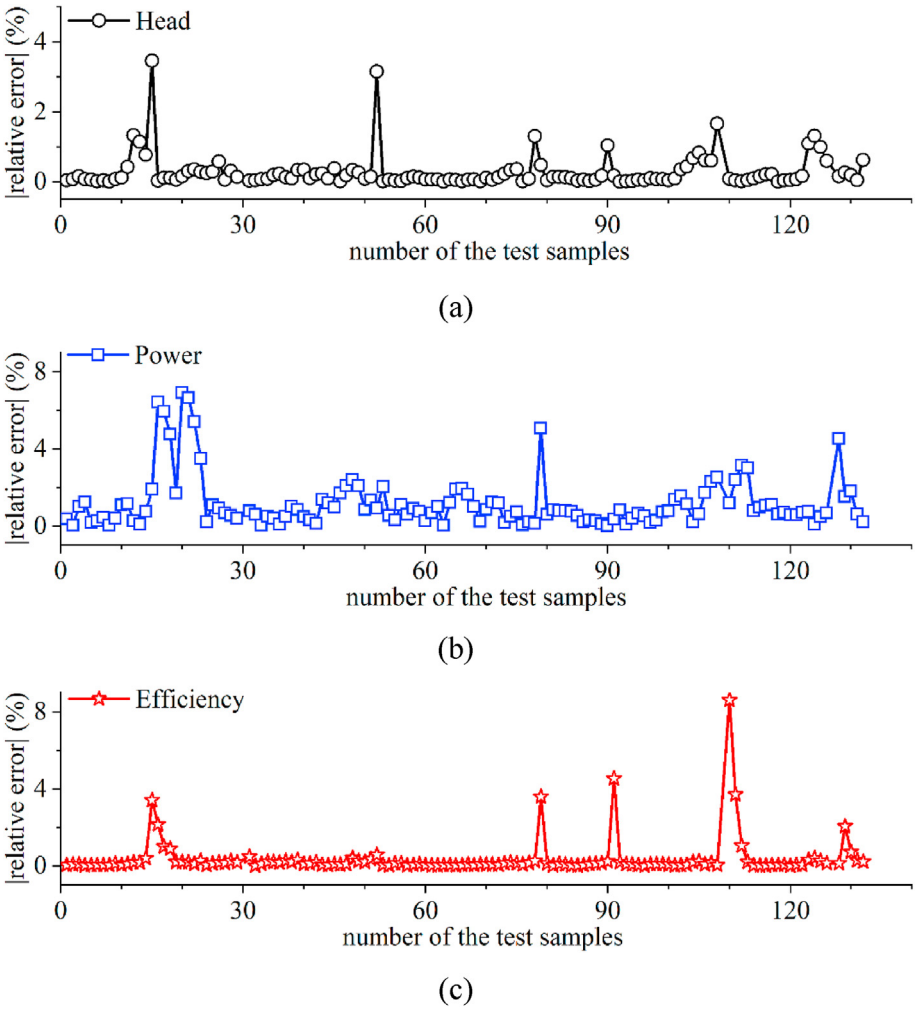

Fig. 10. Absolute relative errors of (a) head, (b) power, (c) efficiency for all the test samples.

Table 1
Statistics of absolute relative errors for all the test samples by the hybrid NN.

	Head	Power	Efficiency
Minimum	0.0012%	0.011%	0.0012%
Maximum	3.5%	6.9%	8.6%
Mean	0.28%	1.2%	0.35%

network structures. The test error is very large in the lower left corner, which demonstrates that the node number for the hidden layers is too small to obtain a satisfied result for the present physical problem. The test error (i.e., the test MSE) becomes smaller with increasing the node numbers for the hidden layers. However, it is over 0.39 when the hidden layers both have 19 nodes. The best neural network structure is marked with white color in Fig. 8, where the node number is 19 for the first hidden layer and 11 for the second hidden layer.

Table 2
The error indices for all the test samples by comparing the predicted values with the experimental data. RMSE is the square of the MSE, as defined in equation (27).

$$\mathrm{RMSE}_j = \sqrt{\frac{1}{p}\sum_{i=1}^{p}\left(y_{i,j} - \hat{y}_{i,j}\right)^2}, j = 1, 2, 3 \tag{27}$$

	Head	Power	Efficiency
MSE	0.0062	8.4E-4	0.020
RMSE	0.079	0.029	0.14

5.2. Predictions for the test samples using the hybrid neural network

The convergence history during the training, validation and test process is shown in Fig. 9 by using the best neural network structure. It is shown that the MSE decreases dramatically without fluctuations and over-fitting during the training, validation and test process, indicating the learning process is converged very well. The best performance is achieved at epoch 1476 as marked with a black circle in Fig. 9.

Furthermore, the predicted values are compared with the experimental values for the test samples in Fig. 10 by using the absolute relative error, which is defined in equation (26).

$$\text{absolute relative error} = \left|y_{i,j} - \hat{y}_{i,j}\right| / y_{i,j}, \; i = 1 \sim 132, \; j = 1 \sim 3 \tag{26}$$

where i represents the i-th test sample; j represents the j-th energy

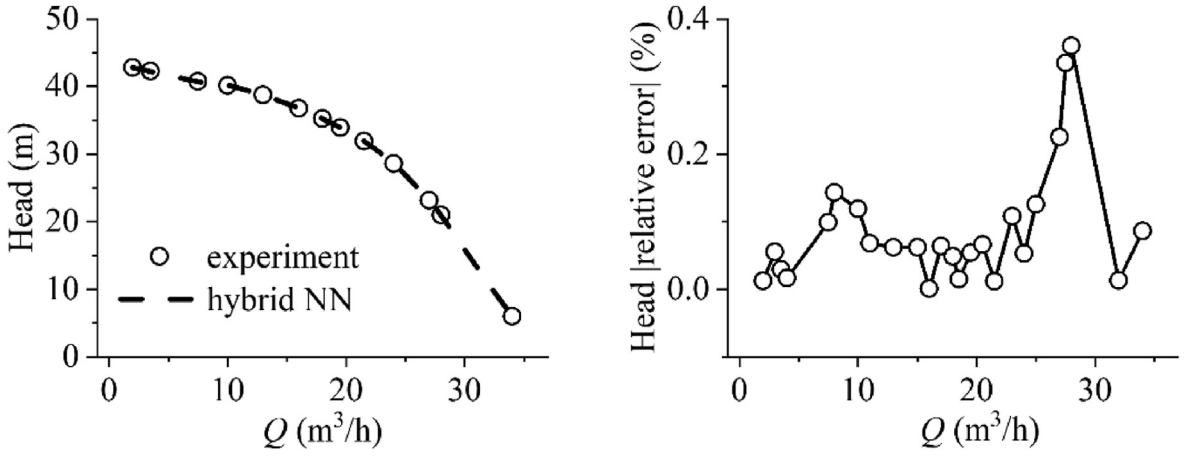

Fig. 11. The head comparisons for one centrifugal pump between the experimental data and the hybrid neural network (NN) predictions.

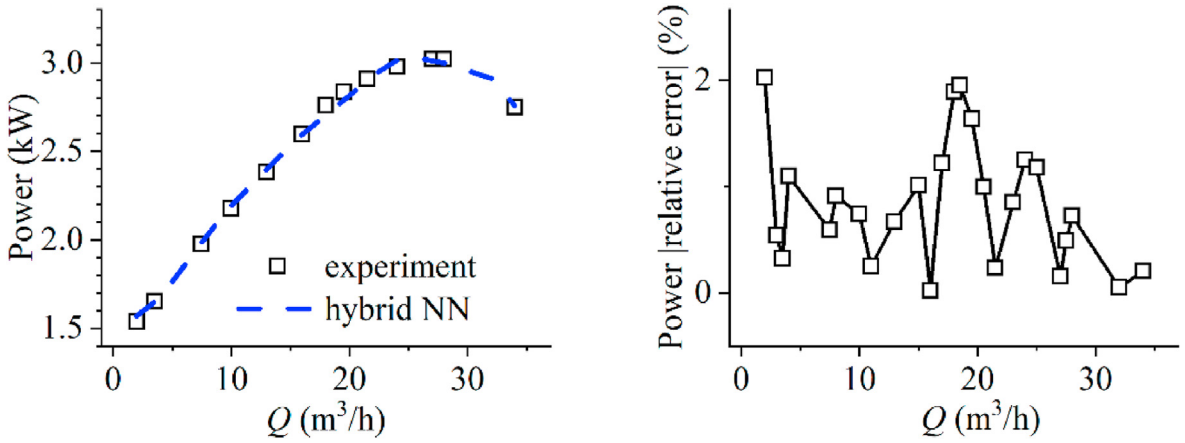

Fig. 12. The power comparisons for one centrifugal pump between the experimental data and the hybrid neural network (NN) predictions.

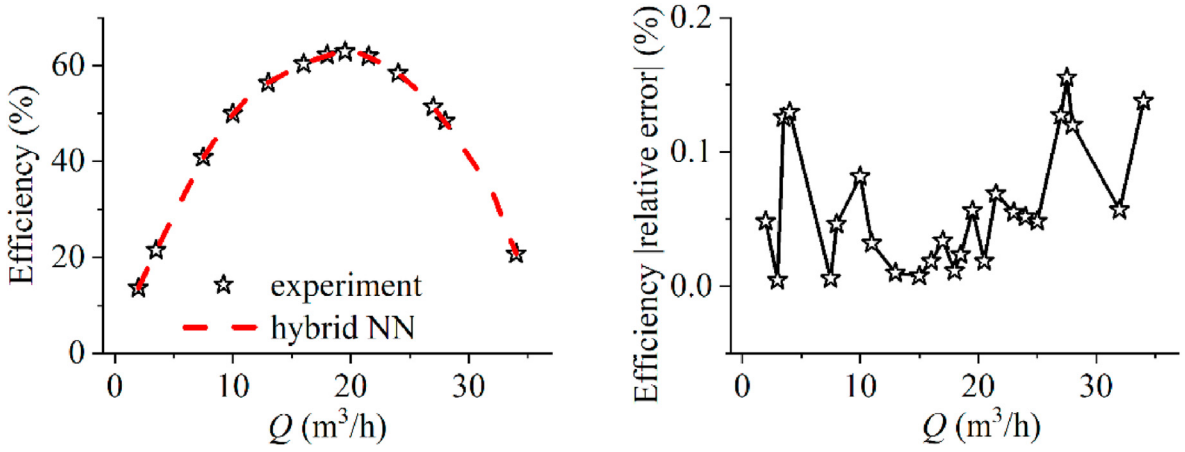

Fig. 13. The efficiency comparisons for one centrifugal pump between the experimental data and the hybrid neural network (NN) predictions.

performance, i.e., head, power, efficiency; $y_{i,j}$ is the target (i.e., the experimental value), $\hat{y}_{i,j}$ is the predicted output.

For the test samples, statistics of absolute relative errors are listed in Table 1. The absolute relative error for the head ranges from 0.0012% to 3.5% with the mean value of 0.28%, the absolute relative error for the power ranges from 0.011% to 6.9% with the mean value of 1.2%, and the absolute relative error for the efficiency ranges from 0.0012% to 8.6% with the mean value of 0.35%. From Fig. 10, most of the absolute relative errors are around the mean values. It is demonstrated that the energy performance (i.e., the head, power and efficiency) is predicted well by using the hybrid neural network.

Table 3
Statistics of absolute relative error for one centrifugal pump.

Method	Item	Head	Power	Efficiency
Original NN	Minimum	0.015%	0.22%	0.0029%
	Maximum	0.72%	4.8%	0.53%
	Mean	0.14%	1.1%	0.13%
Hybrid NN	Minimum	0.0011%	0.026%	0.0043%
	Maximum	0.36%	2.0%	0.16%
	Mean	0.089%	0.84%	0.059%
Linear regression	Minimum	0.35%	0.078%	0.18%
	Maximum	11%	14%	24%
	Mean	3.3%	2.7%	4.9%

Table 2 shows the error indices for all the test samples with the mean-square-error (MSE) and the root-mean-square-error (RMSE). Note that RMSE is the square of the MSE, as defined in equation (25). Note that MSE and RMSE are treated as statistical performance indices without units. The MSE obtained by the hybrid NN is 0.0062, 8.4E-4, 0.020 for the head, power and efficiency, respectively. The RMSE for the head, power and efficiency is 0.079, 0.029, 0.14, respectively.

For the 132 test samples, one of the centrifugal pumps is selected to present the energy performance along with the flow rate Q variations. The geometrical parameters are $D_0 =$ 60mm, $D_1 =$ 56mm, $D_2 =$ 184mm, $b_2 =$ 6mm, $\beta_2 = 14^\circ$, $z =$ 4, $F_t =$ 513mm^2, $Q_d =$ 15m^3/h, $n =$ 2860rpm, and the flow rate Q is varied from $Q = 0 \sim 34$m^3/h. Figs. 11-13 show the energy performance comparisons for this centrifugal pump between the experimental data and the predictions obtained by the hybrid neural network. Statistics of the energy performance for this centrifugal pump are shown in Table 3. During operation conditions for this centrifugal pump, the absolute relative error is 0.0011% ~0.36% for the pump head, 0.026% ~2.0% for the power, and 0.0043% ~0.16% for the efficiency. The mean of the absolute relative error is 0.089% for the head, 0.84% for the power, and 0.059% for the efficiency. The corresponding predictions on the head, power and efficiency are in good accordance with the experimental data when the flow rate ranges from $Q = 0 \sim 34$m^3/h.

5.3. Comparisons with the original neural network

The hybrid neural network proposed in this paper is compared with the original neural network, which directly predict the energy performance without considering the theoretical loss model. Fig. 14 shows the comparisons of the absolute relative error distribution between the original neural network and the hybrid neural network. For the 132 test samples, most of the absolute relative errors are around zero. With the absolute relative error increasing, the number of the test samples is gradually decreased. When looking at the absolute relative error around zero, the hybrid NN number is more than the original NN number. On the other hand, for the absolute relative error around the corresponding maximum, the hybrid NN number is smaller than the original NN number. Therefore, from the perspective of the absolute relative error distribution, the hybrid NN performs better with most of the absolute relative errors around zero.

Table 4 shows the means of absolute relative errors for all the test samples. The means of absolute relative errors obtained by the original NN are 3.9%, 0.97%, 1.3% for head, power, and efficiency, respectively. In contrast, means of relative errors obtained by the hybrid NN are 0.28%, 1.2%, 0.35% for head, power, and efficiency, respectively. Therefore, for the head and efficiency, means of the absolute relative errors from the hybrid NN are smaller than that from the original NN, indicating that the predicted head and efficiency by the hybrid NN are much closer to the experimental data.

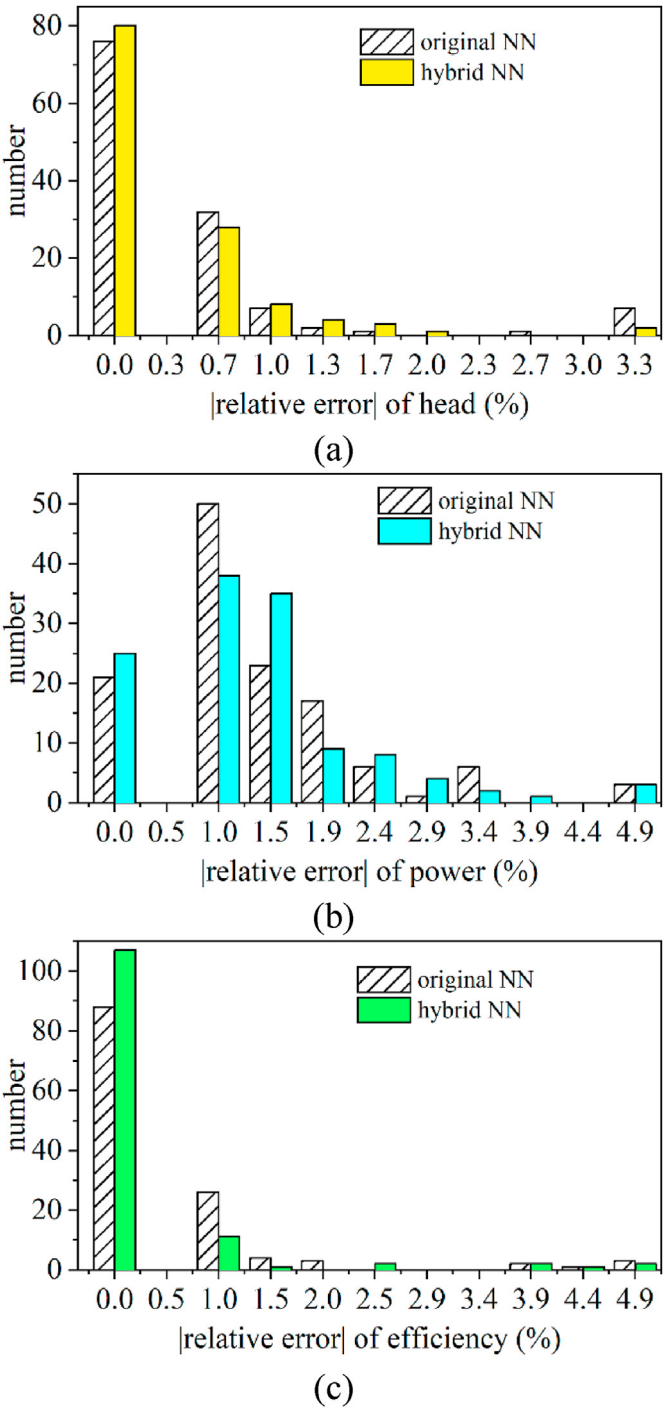

Fig. 14. Comparisons of the absolute relative error distribution for all the test samples between the original neural network and the hybrid neural network.

One centrifugal pump is taken from the test samples to illustrate the energy performance in Fig. 15. The energy performance is predicted well by both the original neural network and the hybrid neural network. The absolute relative errors are shown in Fig. 16 for the head, power and efficiency in the range of $Q = 0 \sim 34$m^3/h. It is illustrated that the absolute relative errors predicted by the original NN are larger than that predicted by the hybrid NN when the flow rate is too small or too large. Take the maximum absolute

Table 4
Means of the absolute relative errors for all the test samples.

Method	Head	Power	Efficiency
Original NN	3.9%	0.97%	1.3%
Hybrid NN	0.28%	1.2%	0.35%
Linear regression	6.6%	2.2%	10%

relative error of the head for example, it is 0.72% and 0.36% for the original NN and hybrid NN, respectively, as shown in Table 3. Besides, the maximum absolute relative error of the power is 4.8% for the original NN and 2.0% for the hybrid NN, and the maximum absolute relative error of the efficiency is 0.53% for the original NN and 0.16% for the hybrid NN. Furthermore, for this centrifugal pump, all of the means of absolute relative errors by the hybrid NN are smaller than that by the original NN.

MSE is used to evaluate the prediction capability of the original neural network and the hybrid neural network, as listed in Table 5. For the original NN, the head MSE is 0.50, the power MSE is 5.9E-4, and the efficiency MSE is 1.3. In contrast, for the hybrid NN, the head MSE is 0.0062, the power MSE is 8.4E-4 and the efficiency MSE is 0.020. As a result, the hybrid NN method shows a better prediction capability, presenting a dramatic decrease by 0.4938 in the head MSE and also a reduction by 1.28 in the efficiency MSE when compared with the original NN.

Moreover, Table 6 shows the RMSE comparisons between the original NN and the hybrid NN based on the whole test samples. For the original NN, the RMSE is 0.71, 0.024, 1.1 for the head, power, efficiency, respectively. For the hybrid NN, the RMSE is 0.079, 0.029, 0.14 for the head, power, efficiency, respectively. As a result, for the hybrid NN, the RMSE is decreased by 0.631 in the head and by 0.96 in the efficiency, although the power RMSE is slightly larger than that of the original NN.

Table 5
MSE of the energy performance (i.e., the head, power and efficiency) for all the test samples.

	Head	Power	Efficiency
Original NN	0.50	5.9E-4	1.3
Hybrid NN	0.0062	8.4E-4	0.020
Linear regression	2.8	0.0036	17

Table 6
RMSE of the energy performance (i.e., the head, power and efficiency) for all the test samples.

	Head	Power	Efficiency
Original NN	0.71	0.024	1.1
Hybrid NN	0.079	0.029	0.14
Linear regression	1.7	0.060	4.1

5.4. Comparisons with the linear regression

There are many advanced data-driven algorithms, but they always require a lot of sample, which is not applicable for present

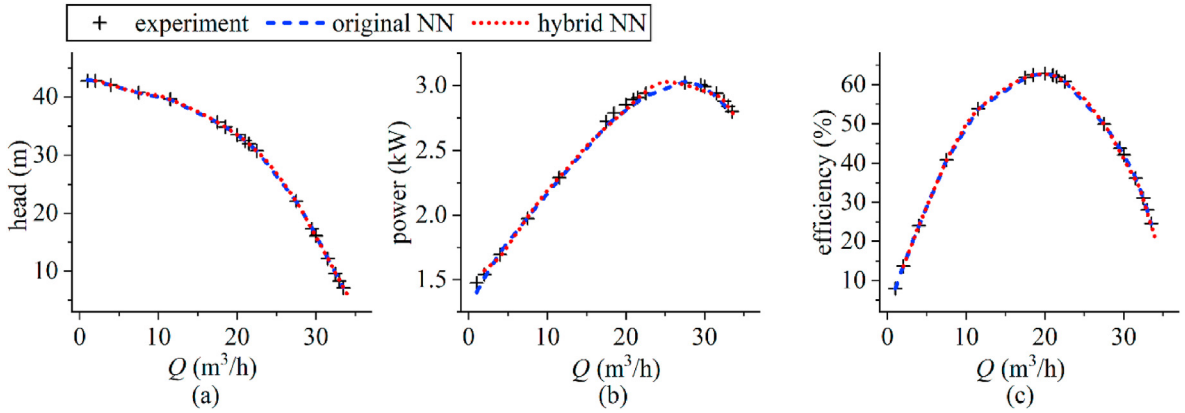

Fig. 15. The energy performance comparisons for one centrifugal pump obtained by using the original neural network and the hybrid neural network.

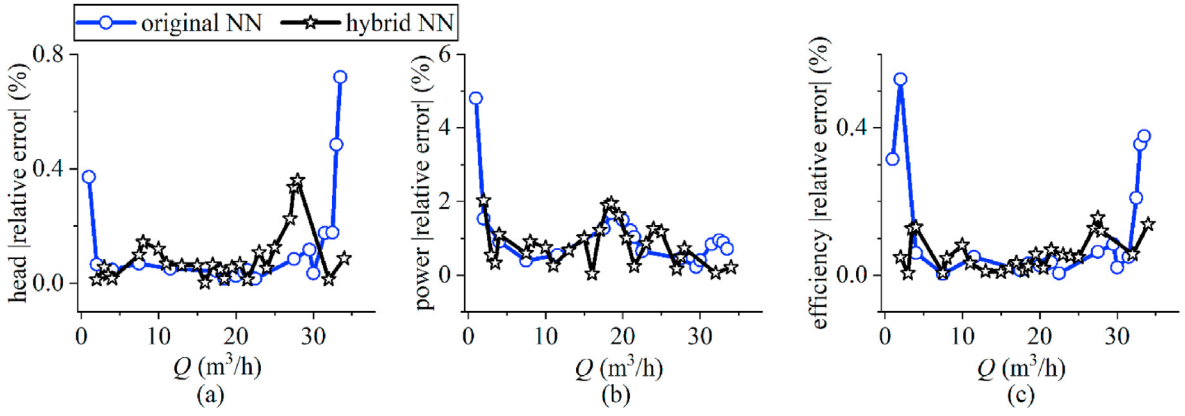

Fig. 16. The absolute relative error comparisons for one centrifugal pump obtained by using the original neural network and the hybrid neural network.

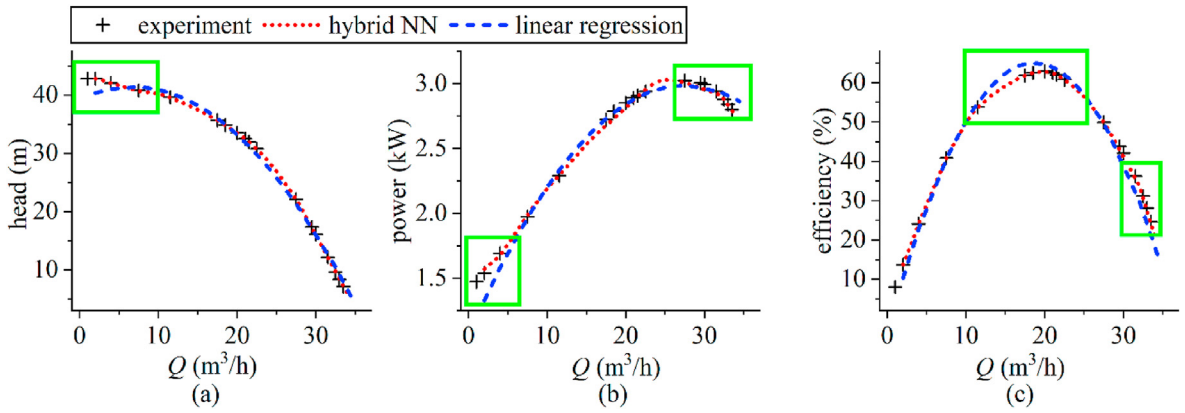

Fig. 17. The variations of the energy performance along with the flow rate (a) head, (b) power and (c) efficiency.

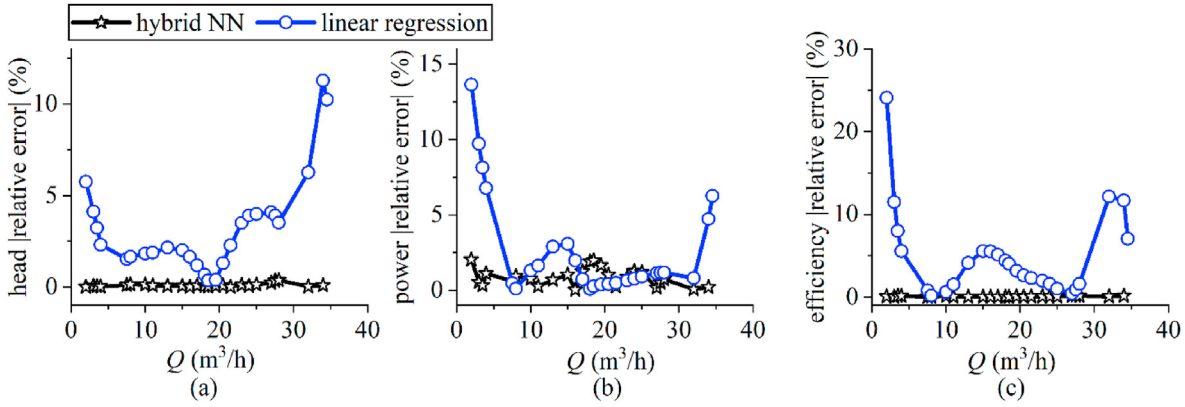

Fig. 18. Comparisons of the absolute relative error obtained by the hybrid neural network and the linear regression method.

physical problem. Based on many previous investigations, the characteristic curves of the energy performance show an approximate linear relation versus flow rate [7,48]. To verify the prediction capability of the hybrid neural network, a multiple quadratic linear regression model [49,50] is carried out for comparison. It is defined as follows,

$$\hat{\hat{y}}_{i,j} = a_{0,i,j} + \sum_{k=1}^{10}\left(a_{k,i,j}x_{k,i,j} + a_{kk,i,j}x_{k,i,j}^2\right) + \sum_{h<k} a_{hk,i,j}x_{k,i,j}x_{h,i,j} \quad (28)$$

where i represents the i-th sample; j means the j-th performance index (i.e., head, power, efficiency); k is the k-th input variable; coefficient a is adjusted to make the predicted value $\hat{\hat{y}}_{i,j}$ close to the target (i.e., the experimental value). As a best linear unbiased estimator, the Ordinary Least Squares (OLS) [50] is adopted herein to calculate the regression coefficient. This method minimizes the sum of squared distances between the true value (i.e. the experimental value) and the fitted responses from the regression model.

The same database obtained from the experiments are used to build the multiple quadratic linear regression model. 309 samples are used for fitting and 132 samples are for testing. Note that the data classification for the linear regression is the same with that for the hybrid neural network. The same centrifugal pump is selected to illustrate the energy performance obtained by the linear regression method.

Fig. 17 shows the variations of the three energy performance along with the increasing flow rate. It is observed that the hybrid neural network can predict the energy characteristics very well when compared with the experiments. In contrast, there are some deviations in the results obtained by the linear regression, especially at the very small flow rates or very large flow rate, as marked with the green rectangles.

The absolute relative errors of the energy characteristics obtained by the hybrid neural network and the linear regression are shown in Fig. 18. The absolute relative error of the linear regression is very large, especially at the very small flow rates or very large flow rates, which is also depicted by Fig. 17. From Table 3, the absolute relative error predicted by the linear regression is varied from 0.35% to 11% for the head, from 0.078% to 14% for the power, and from 0.18% to 24% for the efficiency. As listed in Table 5, the MSE obtained by the linear regression is 2.8, 0.0036 and 17 for the head, the power and the efficiency, respectively, which is increased obviously when compared with the MSEs of the hybrid neural network. As for the RMSE by the linear regression as listed in Table 6, the RMSE is 1.7 for the head, 0.060 for the power and 4.1 for the efficiency. However, the RMSE of the hybrid neural network shows a decrease by 1.621 in the head, 0.031 in the power and 3.96 in the efficiency, indicating the hybrid neural network can perform much better than the traditional linear regression in a wide flow-rate range for multiple centrifugal pumps.

6. Conclusion

This paper aims to accurately and rapidly predict the energy performance (i.e. the head, power and efficiency) of centrifugal pumps. Based on the multiple geometrical parameters and

operation conditions, a hybrid neural network is proposed by incorporating the theoretical loss model into the back propagation neural network, which is a physics-informed neural network and can predict accurate results with a small sample size. Besides, another advantage is that the neural network structure can be automatically optimized. After the hybrid neural network is finally determined, 132 samples are used to test the prediction accuracy of the hybrid neural network by comparing with the experiments, the original neural network, the linear regression. The following conclusions can be drawn:

(1) For the best neural network structure of this problem, the validation error is 0.003, the test error is 0.01, and there are 19 nodes for the first hidden layer and 11 nodes for the second hidden layer.
(2) The energy performance is predicted well by using the hybrid neural network when compared with the experiments. For all the test samples, the mean-square-error (MSE) for the head, power and efficiency is 0.0062, 8.4E-4, 0.020, respectively, and the RMSE for the head, power and efficiency is 0.079, 0.029, 0.14, respectively.
(3) By considering the theoretical loss model, the hybrid neural network shows a better prediction accuracy, especially at the extremely large or small flow rates, demonstrating a dramatic decrease in the head MSE and the efficiency MSE when compared with the original neural network.
(4) When compared with the linear regression method, the RMSE of the hybrid neural network shows a decrease by 1.621 in the head, 0.031 in the power and 3.96 in the efficiency, indicating that the hybrid neural network performs much better than the traditional linear regression in a wide flow-rate range for multiple centrifugal pumps.

Credit author statement

Renfang Huang: Writing - original draft, Conceptualization, Methodology, Zhen Zhang: Investigation, Formal analysis, Wei Zhang: Writing - review & editing, Jiegang Mou: Writing - review & editing, Peijian Zhou: Resources, Formal analysis, Yiwei Wang: Funding acquisition

Declaration of competing interest

The authors declare that they have no known competing financial interests or personal relationships that could have appeared to influence the work reported in this paper.

Acknowledge

The authors would like to gratefully acknowledge National Natural Science Foundation of China (No. 11772340, 11672315 and 52006232), the Science and Technology on Water Jet Propulsion Laboratory (Grant No. 6142223190101).

References

[1] Terreros O, Spreitzhofer J, Basciotti D, Schmidt RR, Esterl T, Pober M, et al. Electricity market options for heat pumps in rural district heating networks in Austria. Energy 2020:116875.
[2] Wang D, Parkinson S, Miao W, Jia H, Crawford C, Djilali N. Online voltage security assessment considering comfort-constrained demand response control of distributed heat pump systems. Appl Energy 2012;96:104–14.
[3] Meesenburg W, Ommen T, Elmegaard B. Dynamic exergoeconomic analysis of a heat pump system used for ancillary services in an integrated energy system. Energy 2018;152:154–65.
[4] Pudjianto D, Djapic P, Aunedi M, Gan CK, Strbac G, Huang S, et al. Smart control for minimizing distribution network reinforcement cost due to electrification. Energy Pol 2013;52:76–84.
[5] Li X, Chen B, Luo X, Zhu Z. Effects of flow pattern on hydraulic performance and energy conversion characterisation in a centrifugal pump. Renew Energy 2019.
[6] Dong Z, Bingyang L, Qintong Z, Jinping L. Thermal performance and energy characteristic analysis of multiple renewable energy complementary heat pump system. Sol Energy 2020;196:287–94.
[7] Liu M, Tan L, Cao S. Theoretical model of energy performance prediction and BEP determination for centrifugal pump as turbine. Energy 2019;172:712–32.
[8] Lee DY, Seo BM, Hong SH, Choi JM, Lee KH. Part load ratio characteristics and energy saving performance of standing column well geothermal heat pump system assisted with storage tank in an apartment. Energy 2019;174:1060–78.
[9] Jin Z, Eikevik TM, Nekså P, Hafner A, Wang R. Annual energy performance of R744 and R410A heat pumping systems. Appl Therm Eng 2017;117:568–76.
[10] Huang RF, Dai YX, Luo XW, Wang YW, Huang CG. Multi-objective optimization of the flush-type intake duct for a waterjet propulsion system. Ocean Eng 2019;187:106172.
[11] Ye W, Luo X, Huang R, Jiang Z, Li X, Zhu Z. Investigation of flow instability characteristics in a low specific speed centrifugal pump using a modified partially averaged Navier–Stokes model. Proc IME J Power Energy 2019;233(7):834–48.
[12] Gu Y, Pei J, Yuan S, Wang W, Zhang F, Wang P, et al. Clocking effect of vaned diffuser on hydraulic performance of high-power pump by using the numerical flow loss visualization method. Energy 2019;170:986–97.
[13] Nam Y, Chae H-B. Numerical simulation for the optimum design of ground source heat pump system using building foundation as horizontal heat exchanger. Energy 2014;73:933–42.
[14] Zhang J, Kong L, Qu J, Wang S, Qu Z. Numerical and experimental investigation on configuration optimization of the large-size ionic wind pump. Energy 2019;171:624–30.
[15] Zeng Y, Yao Z, Gao J, Hong Y, Wang F, Zhang F. Numerical investigation of added mass and hydrodynamic damping on a blunt trailing edge hydrofoil. J Fluids Eng Trans ASME 2019;141(8).
[16] Cheng H, Bai X, Long X, Ji B, Peng X, Farhat M. Large eddy simulation of the tip-leakage cavitating flow with an insight on how cavitation influences vorticity and turbulence. Appl Math Model 2020;77:788–809.
[17] Liu M, Tan L, Cao S. Dynamic mode decomposition of gas-liquid flow in a rotodynamic multiphase pump. Renew Energy 2019;139:1159–75.
[18] Roohi E, Pendar M-R, Rahimi A. Simulation of three-dimensional cavitation behind a disk using various turbulence and mass transfer models. Appl Math Model 2016;40(1):542–64.
[19] Dutta R, Xing T. Five-equation and robust three-equation methods for solution verification of large eddy simulation. J Hydrodyn 2018;30(1):23–33.
[20] Long Y, Long X, Ji B, Xing T. Verification and validation of Large Eddy Simulation of attached cavitating flow around a Clark-Y hydrofoil. Int J Multiphas Flow 2019.
[21] Rodriguez C, Egusquiza E, Santos I. Frequencies in the vibration induced by the rotor stator interaction in a centrifugal pump turbine. J Fluid Eng 2007;129(11):1428–35.
[22] Zhang Y, Zhang Y, Wu Y. A review of rotating stall in reversible pump turbine. Proceedings of the Institution of Mechanical Engineers, Part C. J Mech Eng Sci 2017;231(7):1181–204.
[23] Hao Y, Tan L. Symmetrical and unsymmetrical tip clearances on cavitation performance and radial force of a mixed flow pump as turbine at pump mode. Renew Energy 2018;127:368–76.
[24] El-Naggar MA. A one-dimensional flow analysis for the prediction of centrifugal pump performance characteristics. Int J Rotating Mach 2013;2013.
[25] Deng H, Liu Y, Li P, Zhang S. Whole flow field performance prediction by impeller parameters of centrifugal pumps using support vector regression. Adv Eng Software 2017;114:258–67.
[26] Bing H, Tan L, Cao S, Lu L. Prediction method of impeller performance and analysis of loss mechanism for mixed-flow pump. Sci China Technol Sci 2012;55(7):1988–98.
[27] Kara Omar A, Khaldi A, Ladouani A. Prediction of centrifugal pump performance using energy loss analysis. Aust J Mech Eng 2017;15(3):210–21.
[28] Barbarelli S, Amelio M, Florio G. Predictive model estimating the performances of centrifugal pumps used as turbines. Energy 2016;107:103–21.
[29] Gao Y, Petrie-Repar P. Validation of meanline performance prediction method for radial and mixed flow turbine. Conference Validation of meanline performance prediction method for radial and mixed flow turbine. Institution of Mechanical Engineers, p. 357-372.
[30] Singh P, Nestmann F. An optimization routine on a prediction and selection model for the turbine operation of centrifugal pumps. Exp Therm Fluid Sci 2010;34(2):152–64.
[31] Bellary SAI, Adhav R, Siddique MH, Chon B-H, Kenyery F, Samad A. Application of computational fluid dynamics and surrogate-coupled evolutionary computing to enhance centrifugal-pump performance. Engineering Applications of Computational Fluid Mechanics 2016;10(1):171–81.
[32] Bing H, Cao S. Multi-parameter optimization design, numerical simulation and performance test of mixed-flow pump impeller. Sci China Technol Sci 2013;56(9):2194–206.
[33] Srivastava S, Roy AK, Kumar K. Design analysis of mixed flow pump impeller blades using ANSYS and prediction of its parameters using artificial neural

network. Procedia Engineering 2014;97:2022–31.
[34] Gölcü M. Neural network analysis of head-flow curves in deep well pumps. Energy Convers Manag 2006;47(7):992–1003.
[35] Hinton GE, Salakhutdinov RR. Reducing the dimensionality of data with neural networks. Science 2006;313(5786):504.
[36] Tracey B, Duraisamy K, Alonso J. Application of supervised learning to quantify uncertainties in turbulence and combustion modeling. Conference Application of supervised learning to quantify uncertainties in turbulence and combustion modeling. p. 259.
[37] Zhang Z, Song X-d, Ye S-r, Wang Y-w, Huang C-g, An Y-r, et al. Application of deep learning method to Reynolds stress models of channel flow based on reduced-order modeling of DNS data. J Hydrodyn 2019;31(1):58–65.
[38] Ling J, Kurzawski A, Templeton J. Reynolds averaged turbulence modelling using deep neural networks with embedded invariance. J Fluid Mech 2016;807:155–66.
[39] Huang RF, Luo XW, Ji B, Wang P, Yu A, Zhai ZH, et al. Multi-objective optimization of a mixed-flow pump impeller using modified NSGA-II algorithm. Sci China Technol Sci 2015;58(12):2122–30.
[40] Paeng KS, Chung MK. A new slip factor for centrifugal impellers. Proc IME J Power Energy 2001;215(5):645–9.
[41] Li W-G. Method for analyzing the performance of centrifugal oil pumps. J Fluid Eng 2004;126(3):482–5.
[42] Caridad JA, Kenyery F. Slip factor for centrifugal impellers under single and two-phase flow conditions. J Fluid Eng 2004;127(2):317–21.
[43] von Backström TW. A unified correlation for slip factor in centrifugal impellers. J Turbomach 2005;128(1):1–10.
[44] Liu H, Tan G, Yuan S. Research on calculation of theoretical head of centrifugal pumps. Trans Chin Soc Agric Mach 2006;33:87–90.
[45] Conrad O, Raif K, Wessels M. The calculation of performance maps for centrifugal compressors with vane-island diffusers. Conference the calculation of performance maps for centrifugal compressors with vane-island diffusers. p. 135-147.
[46] Rastegar R, Hariri A. A step forward in studying the compact genetic algorithm. Evol Comput 2006;14(3):277–89.
[47] Wang R, Xu H, Li B, Feng Y. Research on method of determining hidden layer nodes in BP neural network. Computer Technology and Development 2018;28(4):31–5.
[48] Yang S-S, Derakhshan S, Kong F-Y. Theoretical, numerical and experimental prediction of pump as turbine performance. Renew Energy 2012;48:507–13.
[49] Holland PW, Welsch RE. Robust regression using iteratively reweighted least-squares. Commun Stat Theor Methods 1977;6(9):813–27.
[50] Shewhart WA, Wilks SS. Robust statistics: theory and methods. John Wiley; 2006.